CERN/SPSC 98-32
SPSC/M-619
LNGS-LOI 3 Add. 2

THE $N{\cal O}E$ DETECTOR FOR A LONG BASELINE NEUTRINO OSCILLATION EXPERIMENT

G.De Cataldo, C.Favuzzi, P.Fusco, N.Giglietto, F.Loparco A.Rainò, M.N.Mazziotta, I.Panunzio, P.Spinelli
Dip. di Fisica dell'Università di Bari and INFN Sez. di Bari - Italy

A.Margiotta, M.Spurio
Dip. di Fisica dell' Università di Bologna and INFN Sez. di Bologna - Italy

A.Di Credico, A.Grillo, C.Gustavino, S.Mikheyev[1], E.Scapparone
INFN, Laboratori Nazionali del Gran Sasso, Assergi - Italy

P.Bernardini, G.Mancarella, D.Martello, A.Surdo
Dip. di Fisica dell' Università di Lecce and INFN Sez. di Lecce - Italy

R.A.Mukhamedshin, G.T.Zatsepin
Institute of Nuclear Research, Moscow, Russia

V.A.Smotryaev, I.S.Trostin
Institute of Theoretical and Experimental Physics, Moscow, Russia

K.V.Alexandrov, V.A.Chechin, A.P. Chubenko, A.D.Erlykin, F.F.Kayumov, S.K.Kotel'nikov, E.P.Kuznetsov, B.N.Lomonosov, G.I.Merzon, V.A.Ryabov, V.O.Tikhomirov, V.A.Tsarev
P.N.Lebedev Physical Institute, Moscow, Russia

A.M.Baranov, E.T.Gushchin, V.A.Kantserov, A.A.Semak, S.V.Somov
Moscow Engineering Physical Institute, Moscow, Russia

S.V.Golovkine, A.M.Gorine
Institute for High Energy Physics, Moscow, Russia

M.Ambrosio, C.Aramo[2], G.C.Barbarino[*], D.Campana, F.Guarino, A.Lauro, A.Ordine, G.Osteria, V.Palladino, U.Rubizzo
Dip.di Scienze Fisiche dell' Università di Napoli and INFN Sez.di Napoli-Italy

S.Bussino, M.De Vincenzi[3], E.Lamanna
Dip. di Fisica dell' Università di Roma and INFN Sez. di Roma - Italy

G.V.Gavalian, R.L.Kavalov, M.P.Lorikian
Yerevan Physical Institute, Yerevan, Armenia

[*] Contact person
[1] also Institute of Nuclear Research, Russian Academy of Science, Moscow, Russia
[2] also Dip. di Fisica dell' Università di Catania and INFN Catania - Italy
[3] also Dip. di Fisica dell' Università di Roma III - Italy

Abstract

The design of a large underground detector ($N{\cal O}E$) devoted to the search for long baseline neutrino oscillations is presented. The detector is composed by calorimetric modules interleaved with transition radiation (TRD) modules. The basic results of our R&D program are briefly summarized.

The detector has been optimized to be sensitive in the region of $\sin^2 2\theta$ and Δm^2 suggested by the atmospheric neutrino oscillation signal. A simultaneous search for muon neutrino disappearance and appearance of tau and electron neutrinos is possible. The corresponding sensitivities are evaluated on the basis of a complete analysis of Montecarlo events fully simulated and reconstructed in the detector.

1 Conceptual design

The scientific goal of the NOE long baseline (LBL) experiment is the search with the proposed Neutrino to Gran Sasso (NGS) facility for $\nu_\mu \to \nu_\tau$ oscillations and for $\nu_\mu \to \nu_e$ beyond the CHOOZ limit. The major experimental hint for a long baseline ν oscillation search in the regime of low $\Delta \mathrm{m}^2$ ($10^{-2} \div 10^{-3}$ eV^2) comes from the atmospheric neutrino anomalies recently confirmed by SuperKamiokande, MACRO and SOUDAN experiments at the Neutrino 98 conference.

The conceptual design of NOE aims at the discovery of neutrino oscillation by detection of the appearance of ν_τ (by identification of τ decays), of the appearance of ν_e (measuring an excess of events containing an electron) and of the disappearance of ν_μ (measuring a reduction of the apparent NC/CC ratio).

Thanks to this combined approach a stringent double handle (appearance/disappearance) on discovery of $\nu_\mu \to \nu_\tau$ oscillations could be available, especially useful at smaller $\Delta \mathrm{m}^2$. In case of larger $\Delta \mathrm{m}^2$(beyond $\Delta \mathrm{m}^2 = 5 \cdot 10^{-3} eV^2$), besides the search of ν_τ appearance via kinematical cuts, evidence for the energy modulation expected from oscillation for the surviving ν_μ could be collected with adequate statistics.

Many efforts have been done in the last three years to obtain a deeper understanding of the behaviour of NOE detector in presence of oscillations.

The detector has been evolving towards a more sophisticated layout aiming at a better sensitivity to ν_τ appearance. Appeareance searches require the use of higher performance dedicated subdetectors: the basic detector module has to include a sensitive target capable of particle identification, in addition to a calorimeter and muon detector. The total detector tonnage is achieved by a sequence of such identical modules.

Thus two classes of events can be recorded. The first one contains neutrino interactions in a granular and diluted target, where vertex reconstruction, tracking, kinematical analysis and particle identification can take place. The following calorimeter contains the events and measures the total energy. In this sample, detection of ν_τ and ν_e appearance can be achieved. The second class consists of neutrino interactions in the total detector mass. In this sample μ-identification allows, at the same time, the oscillation search in the disappearance channel.

The layout proposed here allows flexibility and good balance between appearance and disappearance search. According to the forthcoming indications from the K2K experiment, upgrades to the detector described here can be foreseen and easily implemented. Some ideas will be presented at the end of this report.

Finally, it is worthwhile to notice that the sensitivity to disappearance increases very weakly as the mass increases ($\propto M^{\frac{1}{4}}$) whereas the granularity coarsens. Therefore to save the ability to perform appearance and disappearance at the same time and to achieve a good event pattern reconstruction, a careful choice of the mass is required.

In this framework the NOE collaboration has developed one possible reference design based on two main subdetector. Further suggestions capable to enhance the detector potential will be welcome.

2 The NOE Detector

According to the previous conceptual considerations, the essential hardware elements of the NOE detector are "light" Transition Radiation Detector (TRD) modules for a total TRD mass of 2.4 kton interleaved with modules of a massive fine grain 5.6 kton calorimeter (CAL). In the TRD target, interaction vertex finding, tracking, e-identification and kinematics reconstruction, are performed. A TRD and a CAL module together, form the Basic Module (BM) of the NOE detector (Fig. 1). The whole 8 kton NOE detector is made of twelve subsequent BM's (Fig. 2).

Particle identification in the TRD and CAL, electron and hadron energy measurements in the CAL and muon energy measurement in the TRD, are the high quality features of this LBL detector. This combination allows a strong rejection of background, making easier identification of oscillation signatures. In particular, in the light TRD target a good reconstruction of neutrino interactions with low hadronic multiplicity (quasi elastic and resonance production) is also possible.

Since the transition radiation is detected by many layers of proportional tubes, the muon energy can be determined by multiple measurements of the energy loss dE/dx, once a muon track has been recognized in the calorimeter. The advantage of such a distributed muon detector is the capability to measure the muon energy even for muon tracks exiting the apparatus from the side walls.

3 The NOE TRD

The main task of the TRD subdetector is to provide a very clean electron identification, to be then followed by an energy measurement in the calorimeter. Besides the ν_e appearance search, ν_τ appearance can be detected

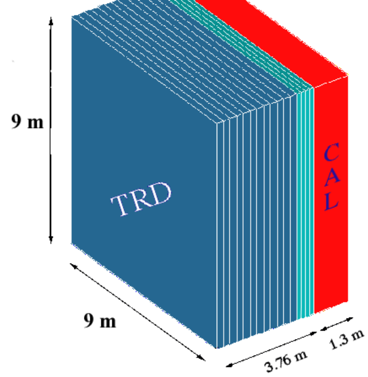

Figure 1: The Basic Module of the NOE detector

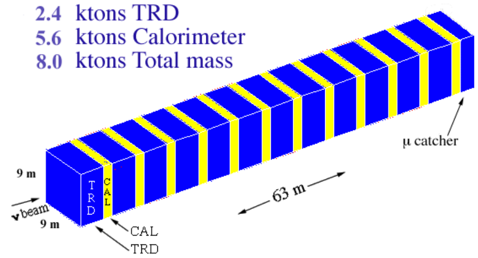

Figure 2: Schematic view of the NOE detector

looking for $\tau \to e$ and $\tau \to \pi$ decays. Due to the low electron background coming from the residual ν_e beam (1% ν_μ), the $\tau \to e\nu\nu$ channel is particularly favourite.

The TRD module consists of 40 vertical layers of 9×9 m^2 surface area, each made of a polyethylene foam radiator ($\rho \sim 35 - 60$ mg/cm^3) and a plane of 320 adjacent proportionaltubes. The tubes have square cross section (3×3 cm^2) alternatively arranged according to the horizontal and the vertical directions and perform the reconstruction of the charged track of the events. The total number of tubes inside a module is 12800. A marble wall of 2.25 cm thickness is set in front of each of the first 32 layers of the TRD acting as a target for the ν. The total length is about 3.9 m.

The last target wall is followed by eight TRD layers, that still provide adequate tracking and identification of secondary particles. The total mass of the 12 basic TRD modules, including the foam and the tube materials, is about 2.4 kton. Each target wall corresponds to 0.22 X_0 (sampling) while the entire TRD basic module corresponds to about 7 X_0 and 1.7 λ_I. The marble facilitates the detection of showering electrons, leaving the pions at minimum of ionization for many layers.

Polyethylene instead of marble can be also considered: in this case each target/sampling would correspond to 0.1 X_0 while the entire module would correspond to about 3 X_0 and 1.8 λ_I. In order to convert efficiently the TR photons inside a tube of 3×3 cm^2 cross section, an Ar (60%) - Xe (30%) - CO_2 (10%) mixture will be used.

The solution of spreading a low density target along the first 32 layers has been adopted for different reasons:

- with a diluted target and good sampling the density of secondary tracks near the production vertex is reduced thus allowing a better multiplicity recognition and space reconstruction of the event.
- the adoption of proportional tube planes, inside the low X_0 target, allows a reasonable fraction of neutral pions (gammas) to travel for a few detection layers without conversion. For example, 65% of π^0 do not convert before the third layer in marble.
- one interaction length along the tracks of charged pions corresponds to 20 layers. Hence it is possible to identify pions as m.i.p.'s in several TRD layers before they interact.

A large volume TRD built for the MACRO detector has been operated at Gran Sasso and extensively studied by one of the groups in the present collaboration.

4 Muon detection

Taking into account that the muons produced in neutrino intereactions at the NGS are in the region of the relativistic rise of dE/dx, the TRD proportional tubes can be used to measure the muon energy in the range 1÷25 GeV, once this particle is identified as a muon in the following calorimetric module. As it is typically done to discriminate hadrons up to 100 GeV/c momentum, using multiple dE/dx measurements in TPCs or proportional chambers, the ionization energy released inside the tubes must be measured by ADCs. In the EPI detector (128 Ar gas samples each of 6 cm depth) the resolution achieved on the ionization energy was ±3%, thus allowing to separate pions from protons at 100 GeV/c. These results were in good agreement with the typical dependence $6.7/L^{0.37}$ of the resolution of gas counters[1] on the total length L.

$\%Fe$ (Weight)	Xo cm	λ_I cm	$<\rho>$ g/cm^3	$<Z>$	E_c MeV
70	5.6	44.5	3.0	15.2	37.

Table 1: Main features of the iron ore (hematite).

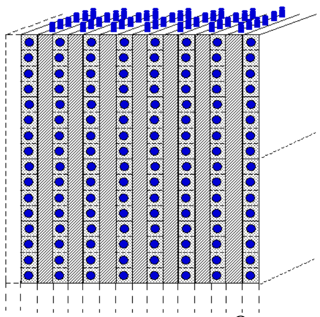

Figure 3: Details of the $N\!O\!E$ calorimeter

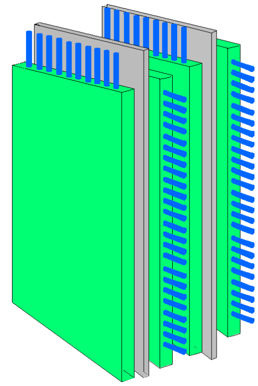

Figure 4: Calorimeter stratigraphy in the crossed fiber planes option.

¿From a study on the Bethe-Block dependence of the specific muon energy loss (ϵ=dE/dx), it turns out that, in order to achieve an energy resolution $\Delta E_\mu/E_\mu$ around the 20%, the resolution $\Delta\epsilon/\epsilon$ on the ionization energy must be $\pm 3\div 4\%$.

Using traces of Kr gas, gain stability can be kept close to 1%. This resolution can be compared to that achieved by using magnetic field technique. A dedicated test beam is planned to check predictions.

In order to measure the muon energy when the neutrino interactions occur in the last TRD and CAL targets, a muon catcher consisting of 32 layers of proportional tubes, equivalent to a TRD basic module, is placed at the end of the $N\!O\!E$ detector.

5 The $N\!O\!E$ calorimeter

Different calorimeter layouts, based on the use of scintillation counters, have been carefully examined. In particular, a sampling iron calorimeter based on scintillating fibers will be described here.

The calorimeter design fulfills the following requirements:

- the thickness has to be dimensioned to absorb events generated in the TRD target.
- The sampling must be $1\div 1.5$ radiation length in order to achieve a good energy resolution.

Several detector prototypes have been built and extensively tested. A present, it turns out that the scintillating fiber solution represent the best choice for the calorimeter.

It is worth noting the high intrinsic granularity of the proposed solution: the average distance between fibers inside the absorber is only a few mm.

5.1 Crossed Fiber-Bars option (C.F.B.)

A preliminary calorimeter set up has been described in the letter of intent submitted to the Gran Sasso Committee in the occasion of a call for proposals for long baseline neutrino experiments[2].

The calorimetric technique of embedding scintillating fibers into an absorber has been developed successfully in the past years. An evolution of such a proven device into a massive detectors is considered in this project. In this option the $N\!O\!E$ calorimeter is composed by 9 m long bars with scintillating fibers parallel to its axis and iron ore radiator distributed inside. Besides radiopurity, the main features of the iron ore absorber are shown in Table 1.

The whole detector is made by alternate planes of crossed calorimetric bars (Fig. 3)[2,3,4].

Assuming read out at both ends, in Table 2 the main features of the calorimeter are shown. All fibers are grouped together at each side of the calorimetric bar, then coupled to single or multipixel photodetector.

Cell (cm^2)	Fe (cm)	layers	λ_I	X_0	$fibers, \lambda_I, X_0$ (number/cell)			elec. chan.
4×4	1.4	12x+12y	5.0	38	28	0.21	1.6	115200

Table 2: Main features of calorimetric bars

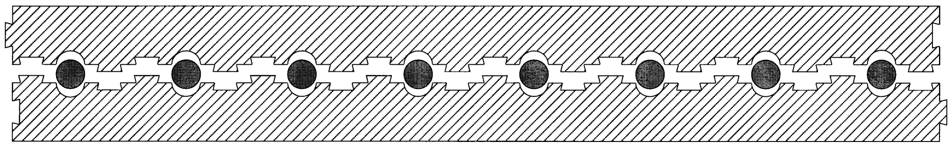

Figure 5: Self-supporting fiber housing for the C.F.P. option

At present the latest production developments of 2 mm diameter scintillating fibers lead to an attenuation length $\lambda = 4.5$ m. Further investigations to improve light yield and attenuation length are in progress.

Using cosmic ray muons, a measurement of the number of photoelectrons as a function of the distance of the impact point from a PMT has been carried out for different number of fibers per bar. Using a low cost and high linearity Hamamatsu R4125 PMT, the total number of photoelectrons from both sides, for 28 fibers in a 4×4 cm^2 bar, is about $26 \pm 15\%$. The most conservative solution for the NOE calorimeter read out is based on commercially available single PMTs or 16 channel Hamamatsu R 5900 00 M16 multianode photomultiplier with 4 mm $\times$ 4 mm pixel size.

Finally we stress that the extreme modularity of the NOE calorimeter allows to assemble the detector elements outside the gallery, greatly improving the construction efficiency.

5.2 Crossed Fiber-Planes option (C.F.P.)

A more sophisticated evolution of the previous layout could be made of crossed fiber planes interleaved with thin absorber iron sheets[4] ($\sim$ 2 mm). Each fiber plane would consist of self-supporting slabs made of extruded iron ore and recycled plastic. The 6.5 mm thin slab would be madeof two identical profiles which provide fiber housing (Fig. 5).

Such a layout allows a finer sampling always in two views, which improves the accuracy of the shower axis determination. Moreover each pattern element is seen at the same time in the X and Y projections. With respect to the previous option the number of fibers per unit thickness is unchanged, but half of the them are oriented in the X direction and half in the Y direction. The number of read out channels will consequently double.

The plastic and iron ore extrusion has been extensively developed and tested by two different factories that manufactured very high quality products with a density up to $\rho = 3.6$ g/cm^3.

6 Detector simulations

The detector simulation is performed using a GEANT 3.21 based Monte Carlo program.

Production of TR photons has been introduced in GEANT whenever a relativistic charged particle ($\gamma \geq 1000$) crosses the radiator. Tables of calculated mean number of photons are used to determine the number of TR X-ray produced (using a Poisson distribution) for given radiator thickness and Lorentz factor γ. The ionization energy by delta rays has also been included.

We assume that the readout of proportional tubes is realized by means of ADCs. A gaussian fluctuation of 12% as overall resolution in the measurement of the pulse heigth as well as the saturation of ADCs at energy deposits of $100\ keV$ in the tube have been included. These assumptions are based on previous tests and measurements in similar conditions.

One of the main task of the TRD target is the strong discrimination between electrons and pions. This feature is the basic requirement to search for τ decay in the most favourite electron channel. In dense calorimeters the e/π shower discrimination is based on complicated algorithms depending on the energy. In TRDs, transition radiation and the presence of a shower give a clean separation of electrons from minimum ioniz-

Particle Type	1 GeV	3 GeV	45 GeV
e	18%	11.5%	9.1%
π	32%	24.4%	19.5%

Table 3: Resolution in the measurement of the total energy released in both sub-detectors for electrons and pions as function of the particle energy.

ing pions. Our simulation shows that averaging the energy loss in the first 10 proportional tube layers, the electron/pion separation is 10^{-3}. Combining the calorimeter information at least 10^{-4} can be reached.

Calorimeter simulation takes into account detector thresholds and non linearities of electronics, Birks saturation in the scintillator, gaussian fluctuations of about 15% around the estimated fiber attenuation length. According to the measured light yield for the mimimum ionizing particle, a mean value of 20 p.e./MeV on each PMT is assumed. The gain of the PMTs is assumed equal to $1.5 \cdot 10^7$, with fluctuation of the order of 30%, coming from both quantum conversion efficiency and electron multiplication.

Simulated electron and pion energy resolutions in the calorimeter are $17\%/\sqrt{(E)}$ and $43\%/\sqrt{(E)}$ respectively. The frequent sampling of scintillating fiber calorimeters appears essential for high resolution energy measurements, as previously extensively proven. Compensation, i.e. equal signal for electrons and hadrons of the same energy, is also achieved.

The energy resolution for electrons and pions emerging from neutrino interactions in the TRD and releasing their energies partially in the TRD and partially in the CAL has has been calculated by Montecarlo (table 3).

7 ν_τ appearance and requirements on the neutrino beams

The rate of ν_τ CC events is given by

$$R_\tau = A \int \sigma_\tau P_{osc} \Phi dE, \tag{1}$$

where E is the neutrino energy, σ_τ the ν_τ CC cross section, P_{osc} the oscillation probability, Φ the muon neutrino flux and A the number of target nucleons in the detector. The search for ν_τ requires that the term $\sigma_\tau P_{osc}\Phi$ is large. Therefore the ν-beam has to provide most of its flux in the energy range where the factor $\sigma_\tau P_{osc}$ is larger. Assuming the mixing of two neutrinos, the oscillation probability is

$$P_{osc} = \sin^2 2\theta \sin^2(1.27\Delta m^2 L/E), \tag{2}$$

where L = 731 km is the distance CERN - Gran Sasso. CC cross section for ν_μ and ν_τ as a function of energy have been adopted comparing different sources and authors. The ν_τ cross section grows slowly with energy above a threshold of about $3.5\ GeV$. For different values of Δm^2 the factor $\sigma_\tau P_{osc}$ has been calculated. It turns out that the optimal energy is about $15\ GeV$ for $\Delta m^2 = 0.01\ eV^2$ and decreases gently with Δm^2 towards a limiting value of about $10\ GeV$[5].

The number of ν_τ CC interactions per 10^{19} protons on target and per kton has been calculated for the 3 reference beams and the corresponding energy distributions of neutrino event rates are shown in Fig. 6. The rate of ν_τ CC interactions is shown in Fig. 7 as a function of Δm^2.

It is worth to mention once again that the average energy of the neutrino beam and the details of its energy spectrum can benefit from further careful optimization. In particular it is desirable to reduce any high energy tail, that does not significantly contribute to the ν_τ rates, whereas it does produce a background of ordinary NC events and of charmed mesons from CC interactions.

This latter is indeed a serious background for any ν_τ appearance experiment. In the NOE detector, and in general in an electronic detector able to apply both topological and kinematical strong cuts, this background can be significantly reduced.

8 τ appearance searches

Tau appearance search is performed on the basis of kinematical identification of τ decay. The $\tau \rightarrow e\nu\nu$ is the favoured channel for this search due to the low background level and the good electron identification capabilities of the TRD. It is worth noting that in the region of atmospheric anomaly the oscillation probability

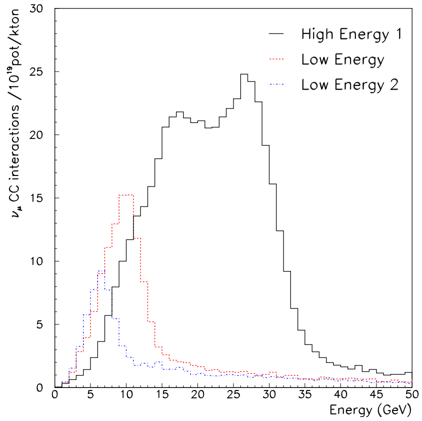

Figure 6: ν_μ CC interaction spectra for different proposed beams.

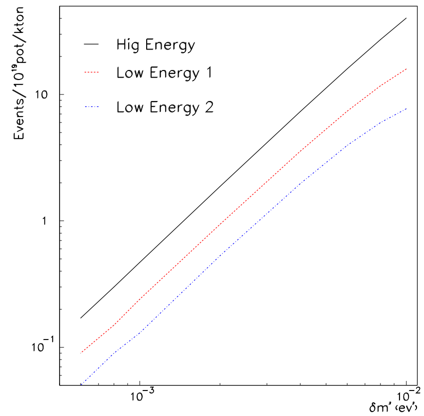

Figure 7: ν_τ CC interactions for different beams vs Δm^2.

is $50 \div 100$ times higher than expected in NOMAD, so that a much lower background rejection power is required.

In order to check the overall *NOE* performances, a complete chain of full event simulation and analysis has been performed. Event generators that include Fermi motion, τ polarization and nuclear rescattering inside the nucleus have been used to simulate deep inelastic, quasi elastic and resonance production events.

Generated events are processed by a GEANT based MonteCarlo in which calorimeter and TRD geometrical set-up are described in great detail, down to a scale of a few mm. Fiber attenuation length, Birks saturation, photoelectron fluctuations and non linearities of the readout electronics for both TRD and calorimeter have been taken in account. DSTs of processed events ($\tau \rightarrow e\nu\nu$, ν_μ NC, ν_e CC and ν_μ CC) have been produced and analyzed.

Electron identification is performed, after selection of fully contained events only, looking for a energy release above a given threshold in the TRD and in the calorimeter readout elements and contained in a $5°$ cone whose vertex is the interaction vertex. The electron direction is reconstructed by weighing the coordinate of each hit by the corresponding energy release. With present algorithms an angular resolution of $0.6°$ and a 180 MeV/c resolution on the measurement of transverse momentum are achieved.

The remaining part of the event is assigned to the hadronic component. The resolution obtained on the measurement of transverse momentum is $420\ MeV/c$.

Topological cuts on the electromagnetic shower are applied to reject ν_μ NC events with π^o faking electrons. In particular the details of the shower, its topology and the absence of signal in the first few layers after the vertex are the basic requirements to reject a fraction of π^o. Work is in progress to improve the reconstruction efficiency and ν_μ NC rejection. Additional cuts are performed to reduce the background due to NC, ν_e CC and ν_μ CC:

- total reconstructed energy $< 20\ GeV$ in the high energy beam and $< 12\ GeV$ in the low energy beam
- electron energy $> 1.5\ GeV$,
- the component Q_{lep} of the electron momentum perpendicular to the hadronic jet direction $> 0.8\ GeV/c$ ($> 0.6\ GeV/c$ in the low energy beam) ,
- transverse mass $M_T = \sqrt{4p_T^e p_T^m \sin^2(\phi_{e-m}/2)} < 2\ GeV$,
- ϕ_{e-h} and ϕ_{m-h} confined to the region below the line shown in Fig. 8. In the transverse plane ϕ_{e-h} is the angle between the directions of the electron and of the hadronic jet and ϕ_{m-h} is the angle between the directions of the missing momentum and of the hadronic jet. Infact for the residual ν_e CC, electron and hadrons are back to back, which is not the case in τ decay where the electron is produced together with two neutrinos.

The first and the last cut mainly reduce the contribution from CC from the contamination of the ν_e in the neutrino beam. The others effectively enhance the rejection of NC background.

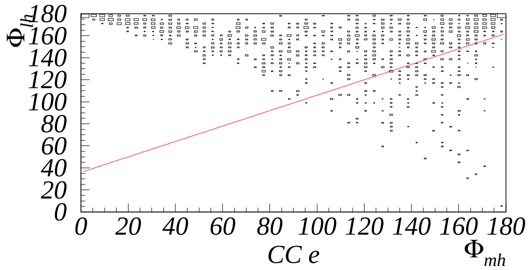

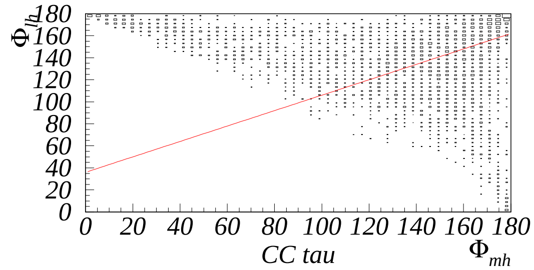

Figure 8: Effects of the ϕ_{e-h} ϕ_{m-h} cut on background (ν_e) and signal (ν_τ).

	Cuts	NC	ν_e CC	$\tau \rightarrow$e
1	Containement	79	67	79
2	Electron finding	13	88	91
3	π_0 rejection	11	88	89
4	$E < 20GeV$	88	45	97
5	$E > 1.5GeV$	65	90	93
6	Q$_{lep} > 0.8GeV$	30	75	75
7	$M_T < 2GeV$	48	75	87
8	ϕ-ϕ	40	13	50

Table 4: Percent efficiency of analysis cuts for the the τ $\rightarrow$e signal and for the main background sources.

The background from charm production comes from the fraction of ν_μ CC events in which the muon is lost and the electron from charm decay is detected. After analysis cuts its contribution is completely negligible.

The efficiency of each individual cut for signal and the main background sources in the high energy beam is reported in Table 4.

Expected number of candidate events, from signal and background, surviving the complete analysis are shown in Table 5. A four years exposure with $4 \cdot 10^{19}$ protons per year is assumed.

Inspection of the columns of the tau yields from appearance and of the muon depletion R in Table 5 suggests that it may be worthwhile to try to design a beam of average energy somewhere in between the two (high and low energy) options considered here so to make both measurements simultaneously significant, in line with the basic concept of the design of the NOE detector.

The minimum detectable oscillation probability is given by

$$P = \frac{1.28 \cdot \sqrt{bck}}{\nu_\mu CC \cdot \eta \cdot B_{\tau \rightarrow e} \cdot \epsilon} \tag{3}$$

where ϵ is the analysis efficiency, B is the branching ratio of the τ decay in electron plus neutrinos and η

	High Energy			Low Energy I		
ν_μ CC	19436			5518		
ν_μ NC	5634			1593		
ν_e CC	110			74		
Δm^2	taus	bkg	R	taus	bkg	R
$7 \cdot 10^{-3}$	27.5	1.74+1.65	0.14	12.3	0.37+1.12	0.36
$6 \cdot 10^{-3}$	20.6	1.83+1.65	0.10	9.6	0.40+1.12	0.30
$5 \cdot 10^{-3}$	14.6	1.87+1.65	0.08	6.9	0.44+1.12	0.23
$4 \cdot 10^{-3}$	9.4	1.92+1.65	0.05	4.6	0.48+1.12	0.16
$3 \cdot 10^{-3}$	5.3	1.97+1.65	0.03	2.7	0.52+1.12	0.10
No Oscillation	-	2.03+1.65	-	-	0.57+1.12	-

Table 5: Analysis results for different beams in the $\tau \rightarrow e$ appearance search as a function of Δm^2. For each beam the expected number of taus after analysis cuts, expected background from ν_μ NC andν_e CC, and the percentage R of oscillated ν_μ in the beam are given.

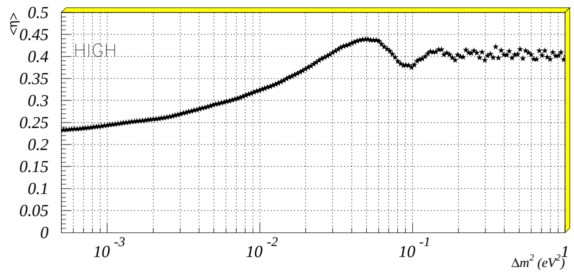

Figure 9: Ratio η of σ_τ/σ_μ averaged on the ν_τ energy spectrum as a function of Δm^2 for the high energy beam.

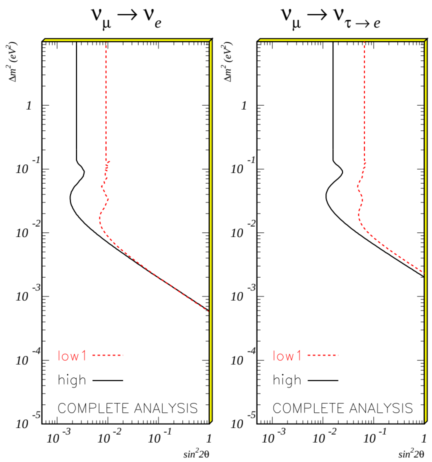

Figure 10: 90% confidence level exclusion plots for appearance searches

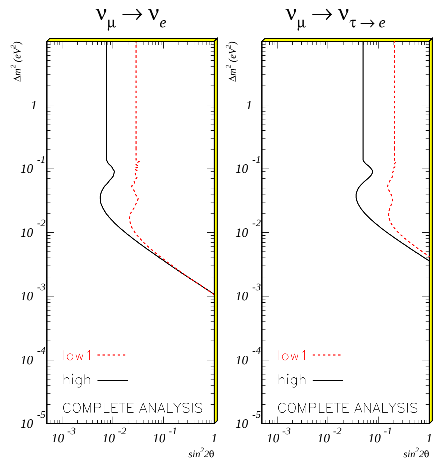

Figure 11: 4σ confidence level exclusion plots for appearance searches

is the ratio of ν_τ and ν_μ cross sections averaged over the ν_τ energy distribution. It is worth noting that the tau energy spectrum depends on the incident ν_μ beam and on Δm^2. Fig. 9 shows this average as a function of Δm^2 for the reference high energy beam. The exclusion plots shown in fig. 10 and 11 are computed by considering the proper η value at each Δm^2.

9 Searches for ν_μ disappearance

A complete analysis/simulation chain has been carried out also for this oscillation search. The identification of charged and neutral current events has been improved by means of a neural network. The algorithm uses several topological, geometrical and calorimetric event parameters as input. The network has been trained with ν_μ CC and NC MonteCarlo events with a neutrino energy uniformly distributed in the range $0 \div 50\ GeV$. The recognition depends essentially on the track length in the event. The energy dependence of efficiencies and fractional contaminations for CC and NC respectively are shown in Fig. 12 and 13.

Further improvements of the recognition algorithm are possible by tuning the neural network and the input parameters. Anyway we think that contaminations and recognition efficiencies are already well known and the measurement is possible with the sensitivity shown in Fig. 14 and 15.

Different beam spectra have been compared. The lower energy beams permit to reach the higher sensitivity in Δm^2 at maximum mixing in the $\nu_\mu \rightarrow \nu_\tau$ oscillation channel. But the sensitivity of the higher energy beam is very close, always within the range $1 \times 10^{-3} \div 2 \times 10^{-3}\ eV^2$.

A near detector to be placed downstream the beam dump should have the primary role to compare neutrino interactions occurring in the near and far locations. In principle any significant difference at the two sites would give firm evidence of neutrino oscillations.

In particular oscillation test could be derived from the comparison, at the near and far locations, of the energy spectra of detected interactions, of the NC/CC ratios, and of the ϕ_{e-h} ϕ_{m-h} correlation for the $\tau \rightarrow$ electron appearance search. The systematic errors due to the non identical near-far ν beam spectra require a careful study.

In order to avoid the systematics due to possible detector differences, both detectors should be built using the same technique and should have the same granularity.

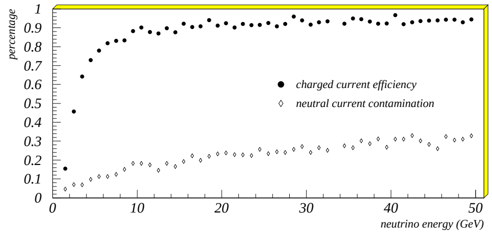

Figure 12: Efficiency and contamination versus neutrino energy.

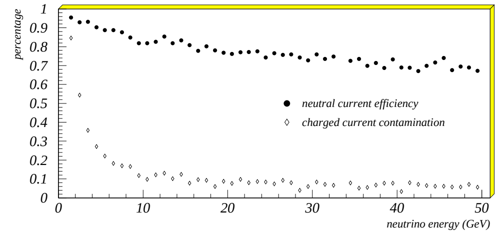

Figure 13: Efficiency and contamination versus neutrino energy.

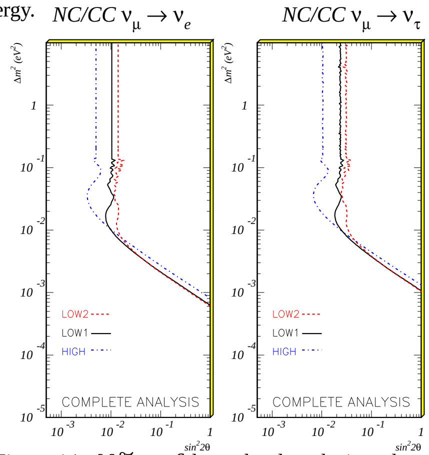

Figure 14: 90% confidence level exclusion plots for disappearance searches

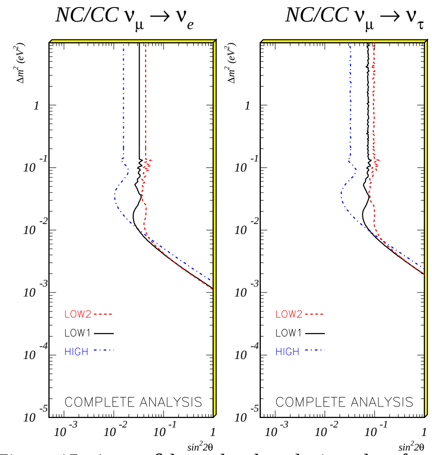

Figure 15: 4σ confidence level exclusion plots for appearance searches

In addition the near detector gives a measure of the ν_e beam contamination. This information is useful to evaluate the background in the electron channel oscillation appearance test.

10 Atmospheric neutrinos

The study of the atmospheric neutrino anomaly can also be performed with our high granularity 8 ktons detector. The ν_e/ν_μ ratio can be measured with *NOE* taking advantage of the clear electron signature in the TRD.

As recently pointed out by many authors, it would be important to measure the flux of atmospheric ν_μ as a function of L/E, where L is the neutrino flight path and E is the neutrino energy. Our detector can track muons with high precision and its capability to measure the hadron energy and direction will provide a good estimate of the neutrino direction and therefore of L .

In addition, these studies could benefit from the rather unique capability of *NOE* to detect a fraction of the protons produced in quasi elastic neutrino events from atmospheric neutrino interacting in the 2.4 Kton of TRD.

The *NOE* technique for muon energy measurement using the proportional tubes of the TRD system was discussed in section 4 and can be complemented by the measurement of the muon range for lower energy muons.

The results of the test beam (scheduled for December 1998 at the CERN PS) is crucial for such analysis. We are confident to be able to quantify in a few months the capability of NOE in the atmospheric neutrino sector.

11 Possible detector improvements and upgrades

The full simulation and analysis of the ν-oscillation on the reference detector provide useful feedback to understand where to address efforts to improve the performance of the detector. Upgrading could be foreseen, studied and implemented eventually on the basis of the forthcoming K2K results.

At present we believe that the calorimeter we have chosen is well balanced in terms of performance and cost. It seems useless to increase the granularity of this device whose main purpose is to measure the energy of the final part of the events. Instead our attention should be focused on the TRD granularity where vertex and kinematical reconstruction of events can be improved to enhance the ν_τ appearance signal.

Some of us have suggested to make the TRD marble targets 'active' by dividing each layer in 2-3 layers interleaved with planes of scintillator strips arranged alternatively according to the X and Y directions and read out by WLS coupled to hybrid photomultipliers (HPD) or electron bombarding CCDs (EBCCD). Strips of about 0.5×0.5 cm^2 cross section ensure a good aspect ratio able to give enough light yield to get high efficiency. Therefore with respect to the reference TRD the sampling could improve by a factor 4 (down to 0.05 X_0), thus allowing a higher fraction (90%) of gammas from neutral pions decays to travel for a few active layers without conversion. Hence, very powerful e/π^0 discrimination and high granularity event topology can contribute to reduce the NC background close to zero. The kinematical reduction of ν_e CC background would also take advantage of the higher granularity. Preliminary calculations indicate that the background shown in table 5 for the ν_τ appearance analysis based on the reference detector can be reduced by a factor of 2.

12 Logistics and costs

The NOE detector can be located in hall B of the Gran Sasso Laboratory. Like MACRO, NOE consists of 12 modules (TRD+CAL). Such a configuration allows to reuse the gas system and the distribution pipelines for the TRD proportional tubes. In addition the possibility to reuse part of the mechanical and electronic equipment has been considered. The total estimated saved cost is 4 M dollars.

The breakdown of the costs for the proposed detector configurations and the total cost of NOE are shown in table 6. Due to the fact that TRD cost/kton is even lower than calorimeter cost/kton, the use of two subdetectors does not add any additional cost with respect to a less powerful homogeneous detector.

The present year 1998 has been devoted to build a prototype 1:1 in thickness of the basic module TRD+CAL to test at PS in december. Several results concerning e/π discrimination, energy resolution, muon energy resolution and calibrations for Montecarlo simulation will be achieved.

	Cost (M dollars)
Calorimeter (CFB)	
Fibers	6
Absorber (bars and Iron ore)	2
Photodetector system	7
Readout and ADCs	1
Total	**16**
CFB calorimeter cost/kton	2.8
Calorimeter (CFP)	
Fibers	7.5
Absorber (Extrusions and Iron)	5.5
Photodetector system	5
Readout and ADCs	2
Total	**20**
CFP calorimeter cost/kton	4.6

	Cost (M dollars)
TRD	
Proportional Tubes	3.5
Absorber	0.5
Radiator (Foam)	0.1
Readout and ADCs	1.5
HV	0.2
Gas system	0.6
Total TRD	**6.4**
TRD cost/kton	2.7

	Cost (M dollars)
Mechanichs	2
Trigger, ACQ	2
Total	**4**

Detector config.	Total cost (M dollars)	Total cost with MACRO saving (-4) (M dollars)
TRD + CFB	26.4	22.4
TRD + CFP	30.4	26.4

Table 6: Details of sub-detectors costs

References

1. I. Lehraus et al., *Nucl. Instrum. Methods* A **153**, 347 (1978); I. Lehraus et al., *Nucl. Instrum. Methods* **217**, 1983 (.)
2. G. Barbarino et al., "NOE Atmospheric and long baseline Neutrino Oscillation Experiment" INFN/AE-96/11 (1996)
3. M.Ambrosio et al., NIMA **363**, 604 (1995)
4. G. Barbarino et al., "The NOE detector for a long baseline neutrino oscillation experiment" INFN/AE-98/09 (1998).
5. G. Barbarino et al., "Requirements from NOE for ν_τ appearance in the NGS ν beam" NOE Note 9/98